Supplementary Material for "Assessing Earthquake potential and Fault Activity from a Dense 3D Geodetic Velocity field in Hispaniola"

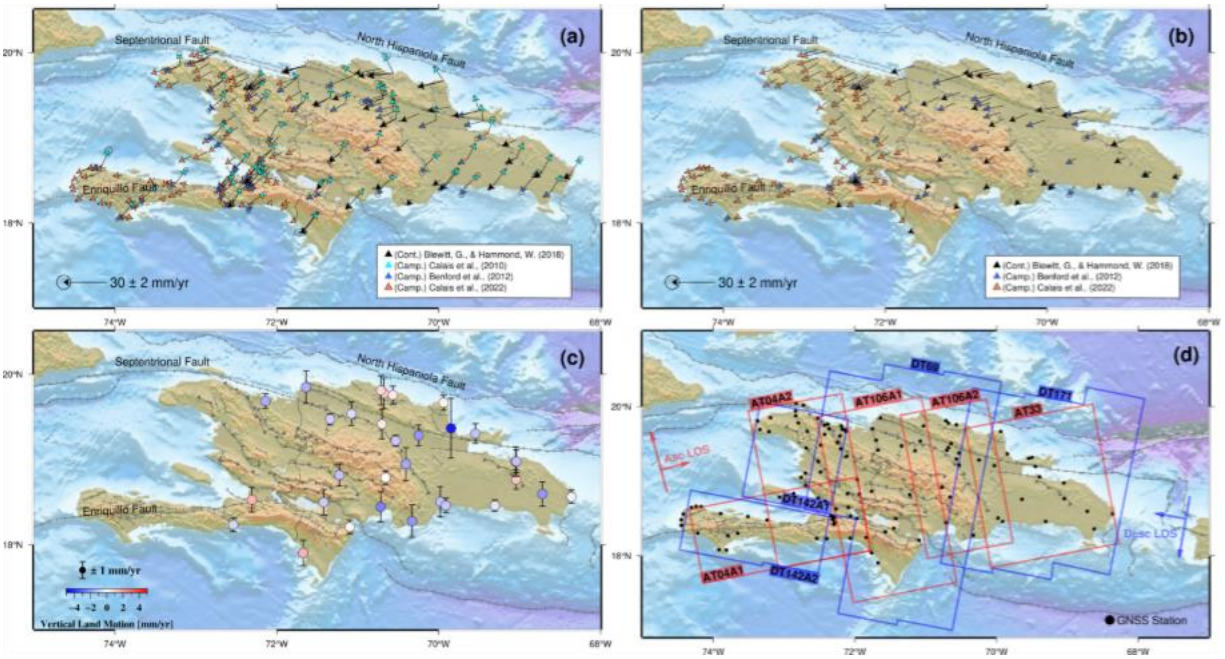

Figure 1. Geodetic measurements were used in this study. (a) Original GNSS velocity field. The black arrows mark 32 continuous GNSS velocity fields from the Nevada Geodetic Laboratory (UNR) (Blewitt et al., 2018). The cyan arrows are from Calais et al. (2010), blue arrows are from Benford et al. (2012), and orange arrows are from Calais et al. (2022). Each dataset is referenced to its own reference frame. **(b) Updated GNSS horizontal velocity field.** The black arrows mark 32 continuous GNSS velocity fields from the Nevada Geodetic Laboratory (UNR) (Blewitt et al., 2018). The blue arrows are from Benford et al. (2012), and orange arrows are from Calais et al. (2022). **(c) Updated GNSS vertical velocity field.** Red represents uplift, and blue represents subsidence. **(d) InSAR tracks**. Red frames are ascending track; blue frames are descending tracks.

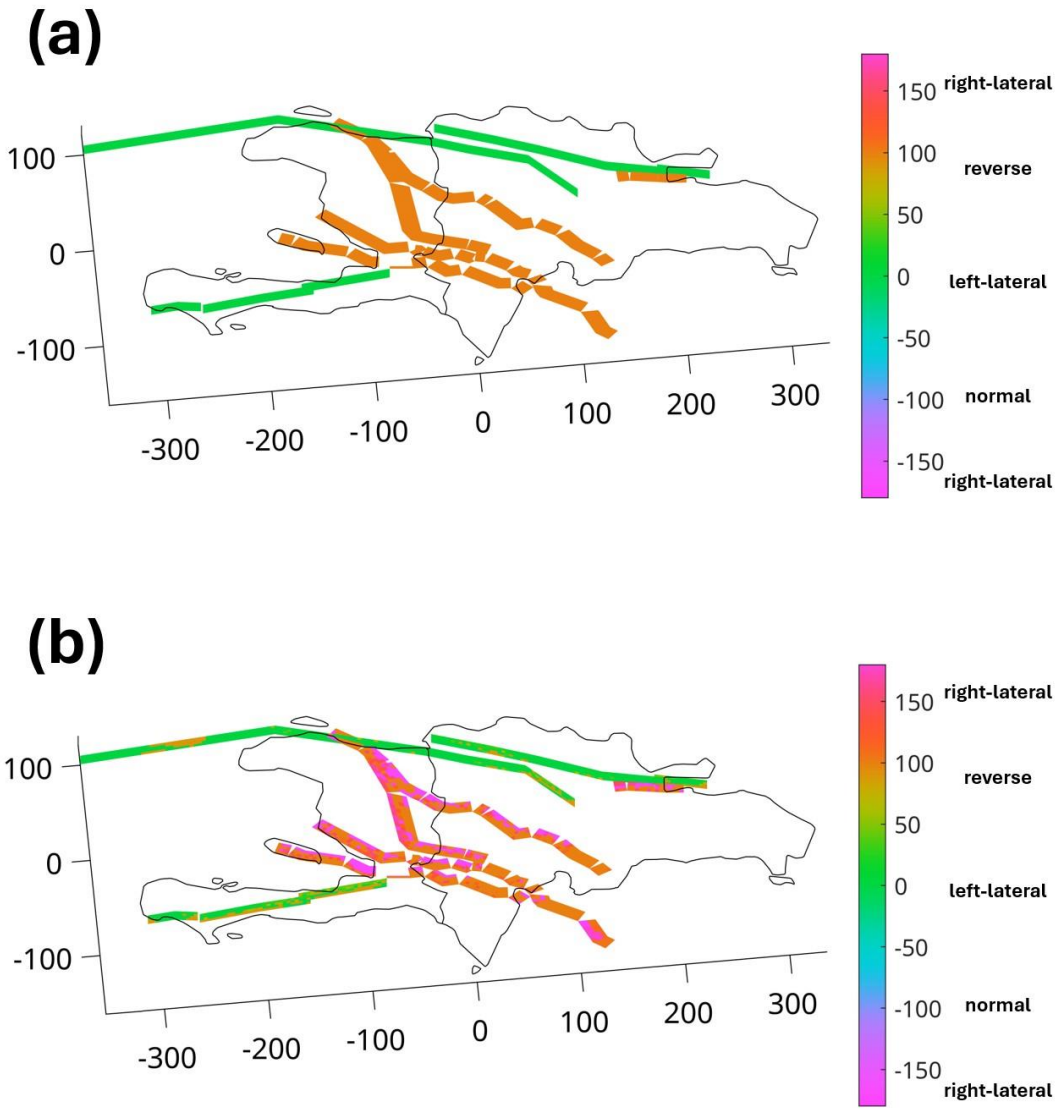

Figure 2. Distribution of fault rake angles (degrees). (a) Initial prior constraints used in the modeling framework. (b) Optimized rake configuration resulting from the inversion.

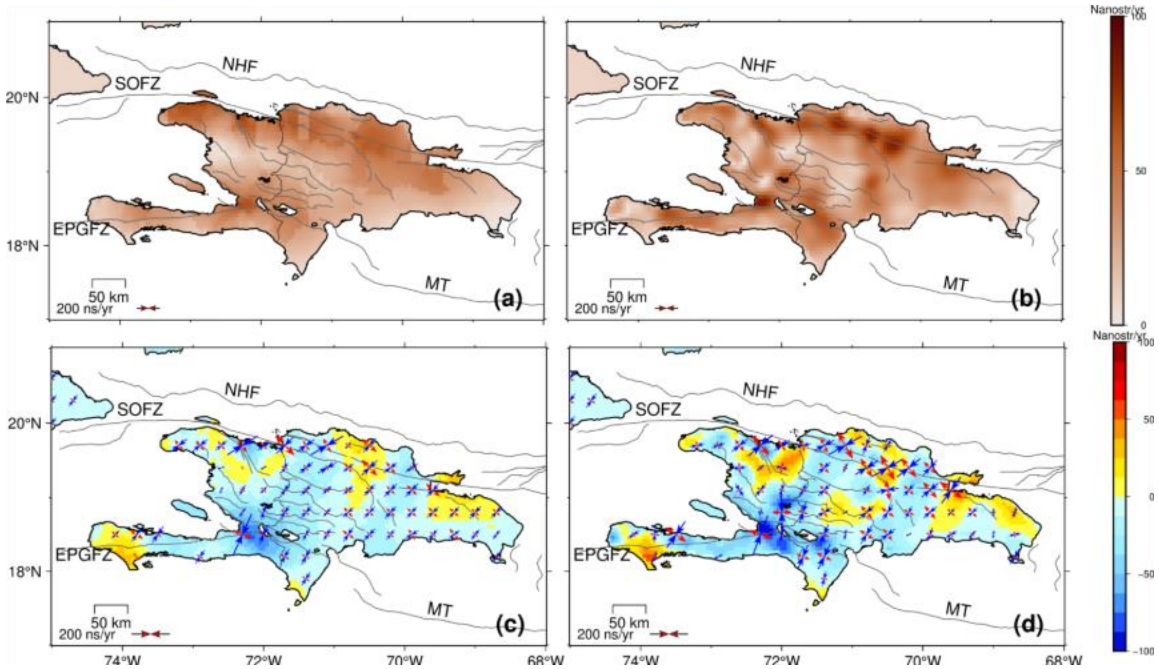

Figure 3. Strain rate results including GNSS-only (a, c) and combined GNSS+InSAR (b, d) results. (a, b) Maximum shear strain rates. (c, d) Dilatation rates. Positive indicates extension, and negative denotes contraction.

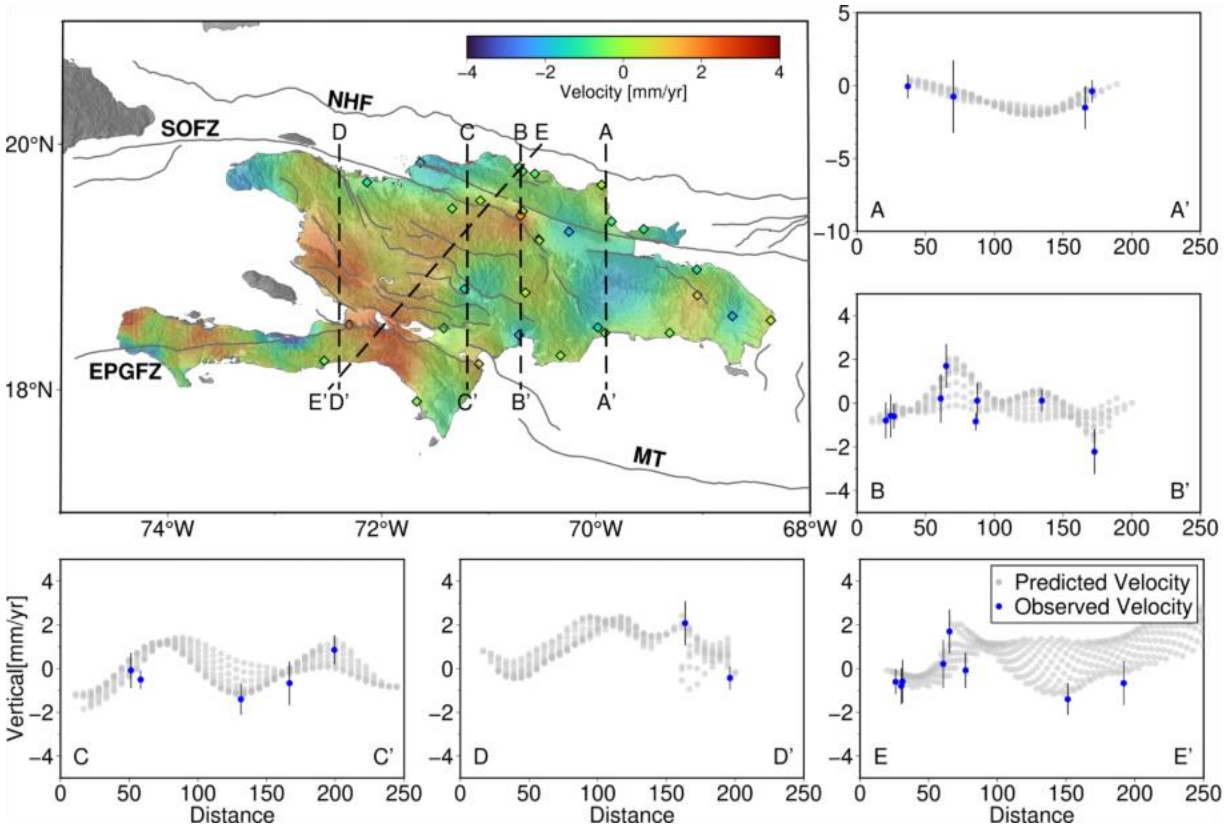

Figure 4. Modeled vertical velocity field and cross-sectional profiles. The main panel displays modeled vertical velocities, with fault traces indicated by solid gray lines. Diamonds represent continuous GNSS stations, colored by their respective vertical velocities. Dashed black lines indicate the locations of velocity profiles AA' through EE', which are detailed in the subpanels. Within these profiles, gray dots represent predicted velocities, while blue dots signify observed GNSS vertical velocities with 1-sigma error bars.

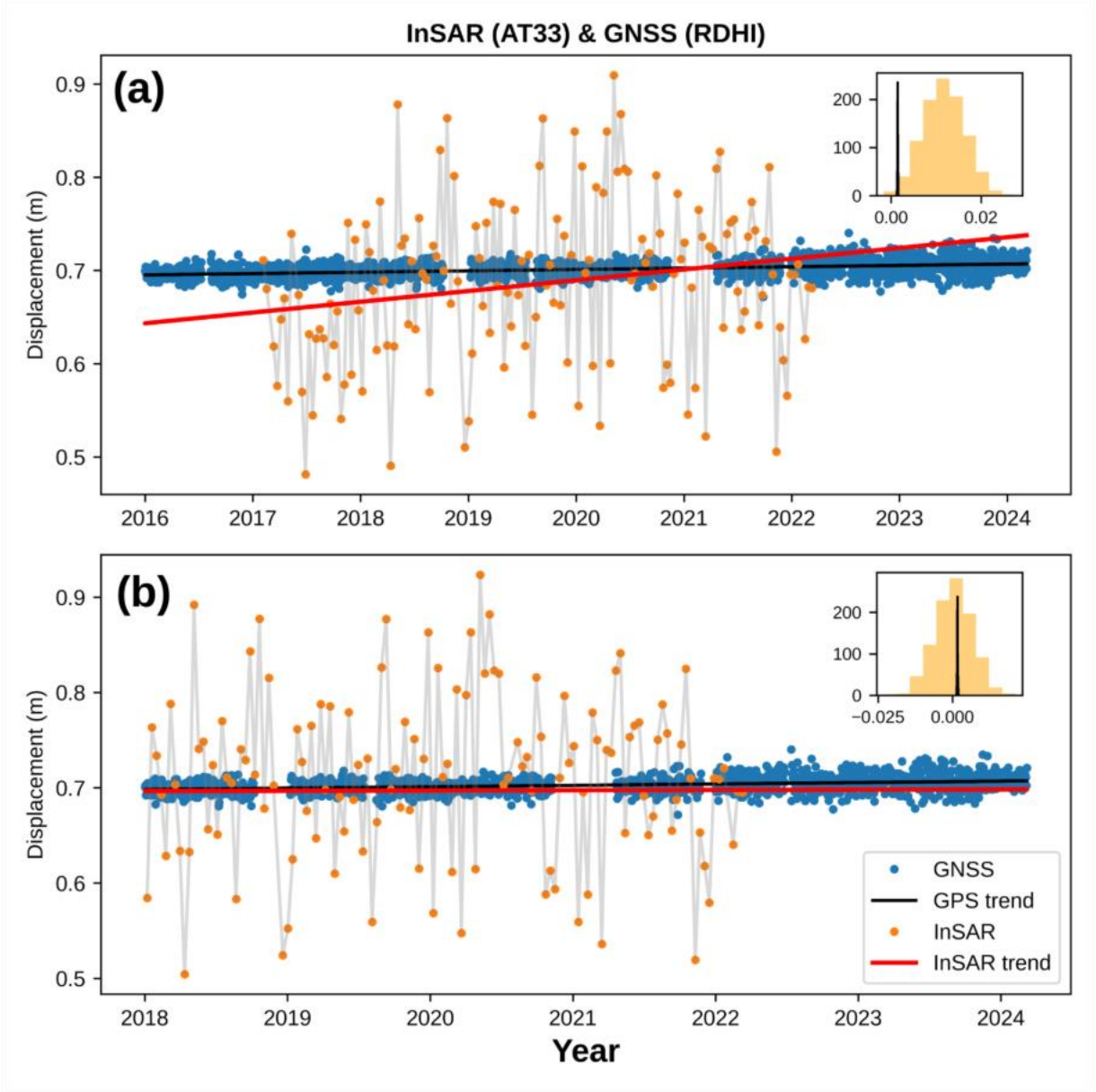

Figure 5. Uncertainty evaluation of InSAR and GNSS time series. (a) Comparison of vertical displacement between GNSS station RDHI and InSAR Ascending Track 33 for the 2016–2024 period. **(b)** Comparison using a restricted 2018–2025 timeframe. Inset histograms show the distribution of velocity uncertainties derived from bootstrap analysis, with InSAR represented in orange and GNSS in black.

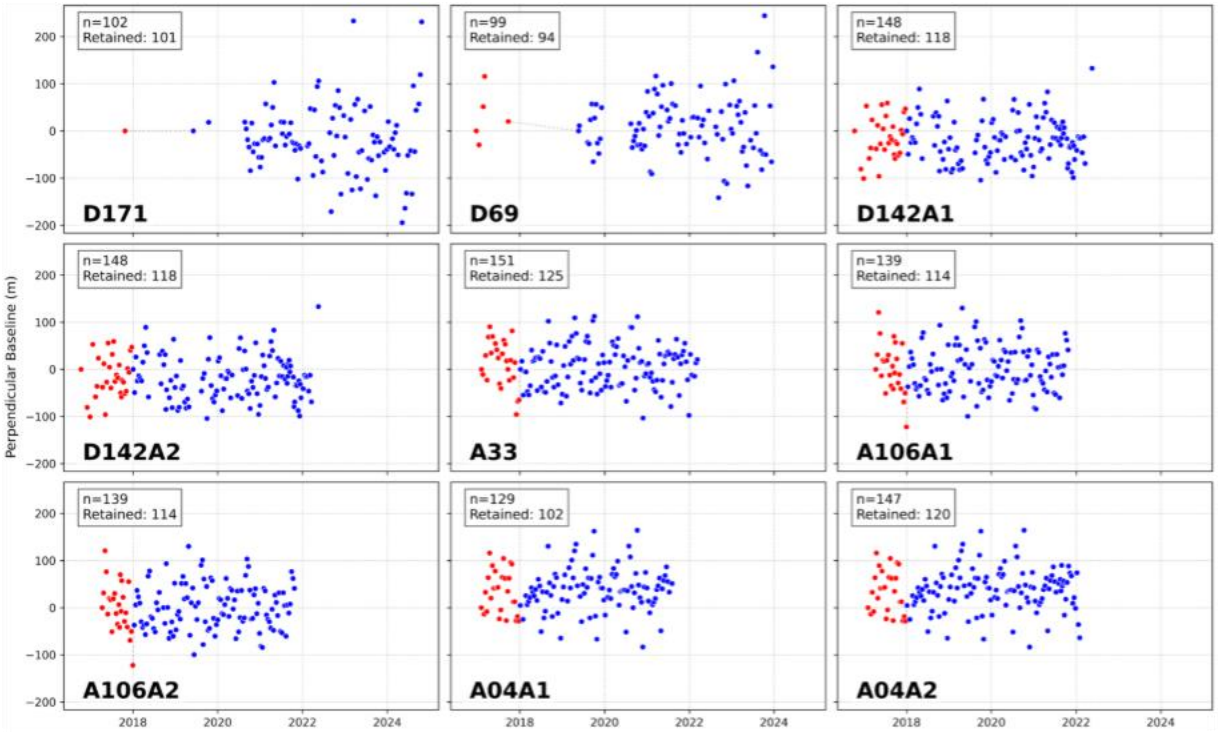

Figure 6. InSAR baseline. The x-axis denotes acquisition year and the y-axis represents the perpendicular baseline (meter). Blue dots indicate the acquisitions used in this study, while red dots represent scenes prior to 2018 that were excluded from the analysis. Box in the upper-left corner indicates the total number of acquisitions (n) and the final subset used (retained). The satellite track number is provided in the lower-left corner.

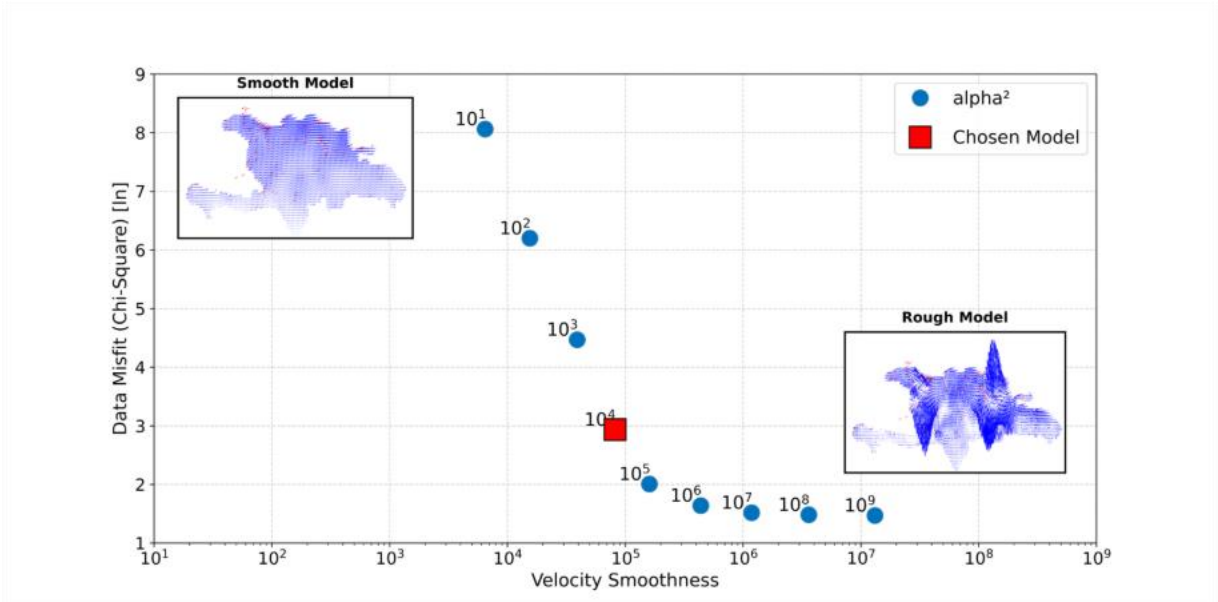

Figure 7. L-curve of the smoothness (k^2) decision. The blue dots represent different values of alpha^2, and the red square is the final model (10^4) what we chose. The smooth model corresponds to results obtained using a smaller alpha^2, while the rough model is the result of a higher alpha^2.

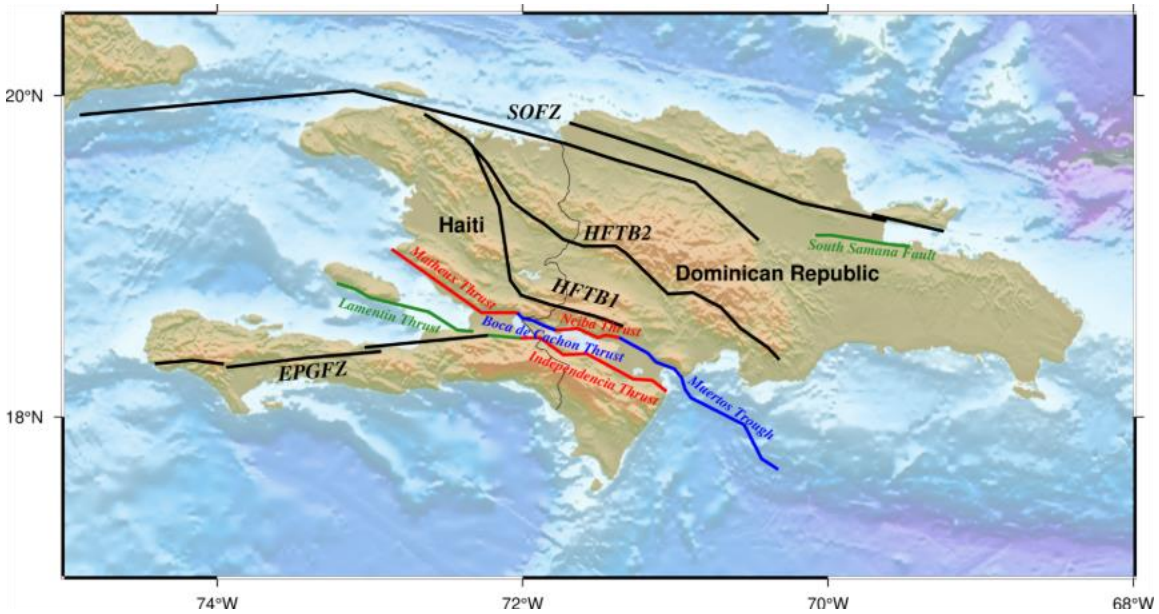

Figure 8. Fault segments setup. EPGFZ: Enriquillo-Plantain Garden Fault zone; SOFZ: Septentrional-Oriente Fault zone; HFTB: Haitian Fold and Thrust.

Table 1. Total moment rate for each strain rate method.

Method	Depth [km]	Moment rate [x10^{18} N m/yr]	Equivalent Magnitude [Mw]
Gpsgridder (Sandwell & Wessel, 2016)	20	4.8	6.42
	30	7.2	6.54
	40	9.6	6.62
Geostats – Gaussian (Maurer & Materna, 2023)	20	4.85	6.42
	30	7.28	6.54
	40	9.71	6.62
loc_avg_grad (Huang et al., 2022)	20	5.09	6.44
	30	7.64	6.56
	40	10.18	6.64
Wavelets (Tape et al., 2009)	20	3.72	6.35
	30	5.58	6.46
	40	7.44	6.55
Average	**20**	**4.615**	**6.41**
	30	**6.925**	**6.53**
	40	**9.233**	**6.61**